Cell

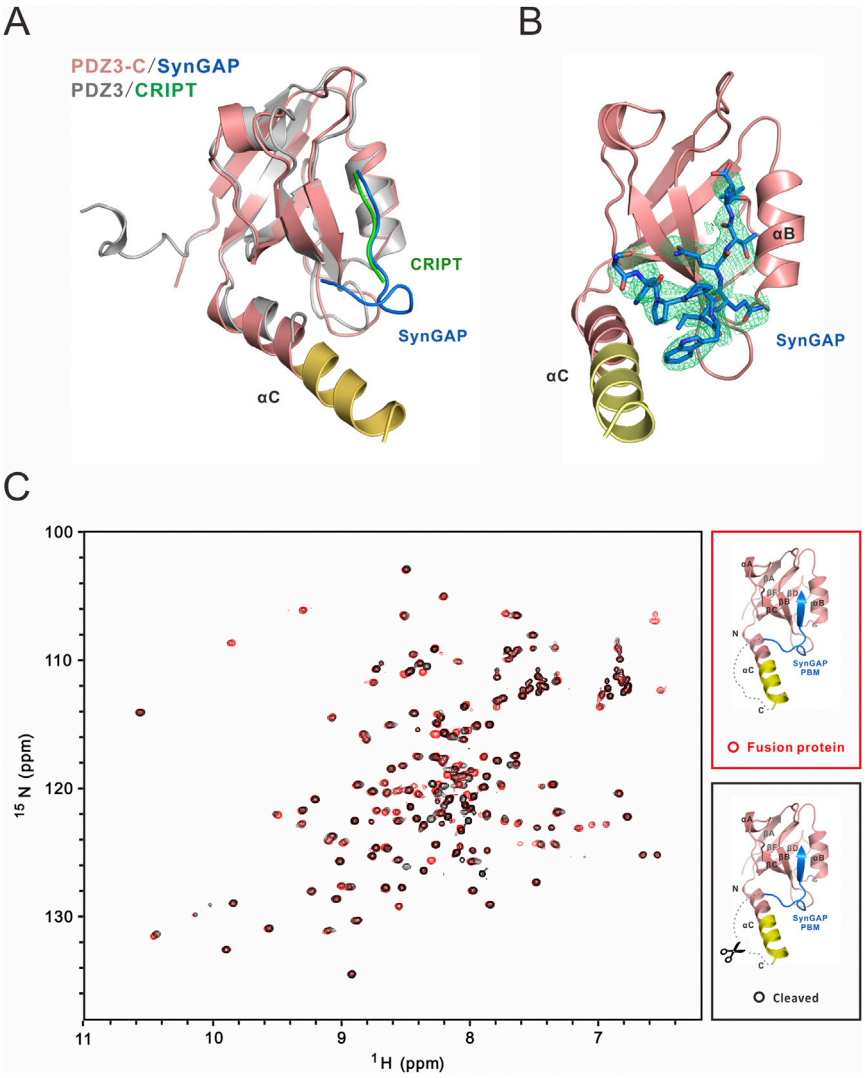

Figure S1. Structure of the PSD-95 PDZ3-C/SynGAP PBM Complex, Related to Figure 1

(A) Comparison of the structure of the PSD-95 PDZ3-C/SynGAP PBM complex with that of the PSD-95 PDZ3/CRIPT complex.

(B) The 2Fo-Fc omit map of the SynGAP PBM peptide in the complex with PSD-95 PDZ3-C. The map is countered at the level of 1.0σ.

(C) An overlay plot of the ^{1}H, ^{15}N-HSQC spectra of the PSD-95 PDZ3-C/SynGAP PBM fusion protein before and after thrombin cleavage.

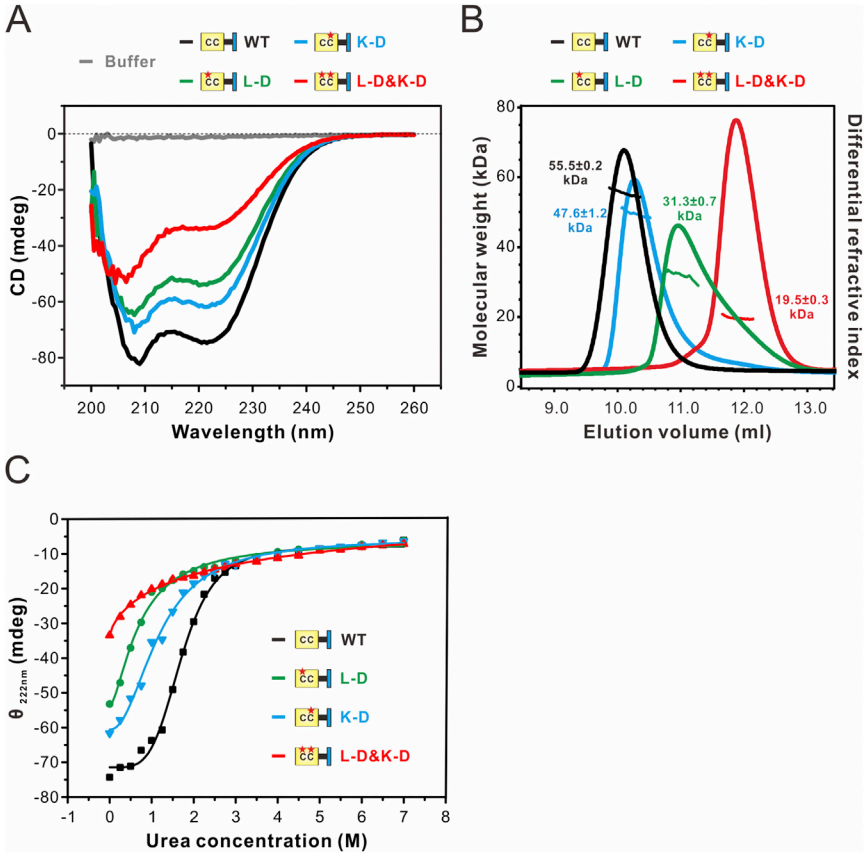

Figure S2. Characterization of Various SynGAP Trimer-Disruption Mutations on the Formation of the SynGAP CC-PBM Trimer, Related to Figure 2

(A) CD spectra showing that two single point mutations decrease the α-helical content of SynGAP CC-PBM, and the combined double point mutations (L-D&K-D) further decrease the helical content of the protein.

(B) FPLC-coupled static light-scattering analysis showing that the point mutations weaken or even disrupt the trimer formation of SynGAP CC-PBM.

(C) CD spectra-based urea-induced denaturation assay showing that the point mutants are less stable than WT, with the double point mutant (L-D&K-D) having the lowest stability.

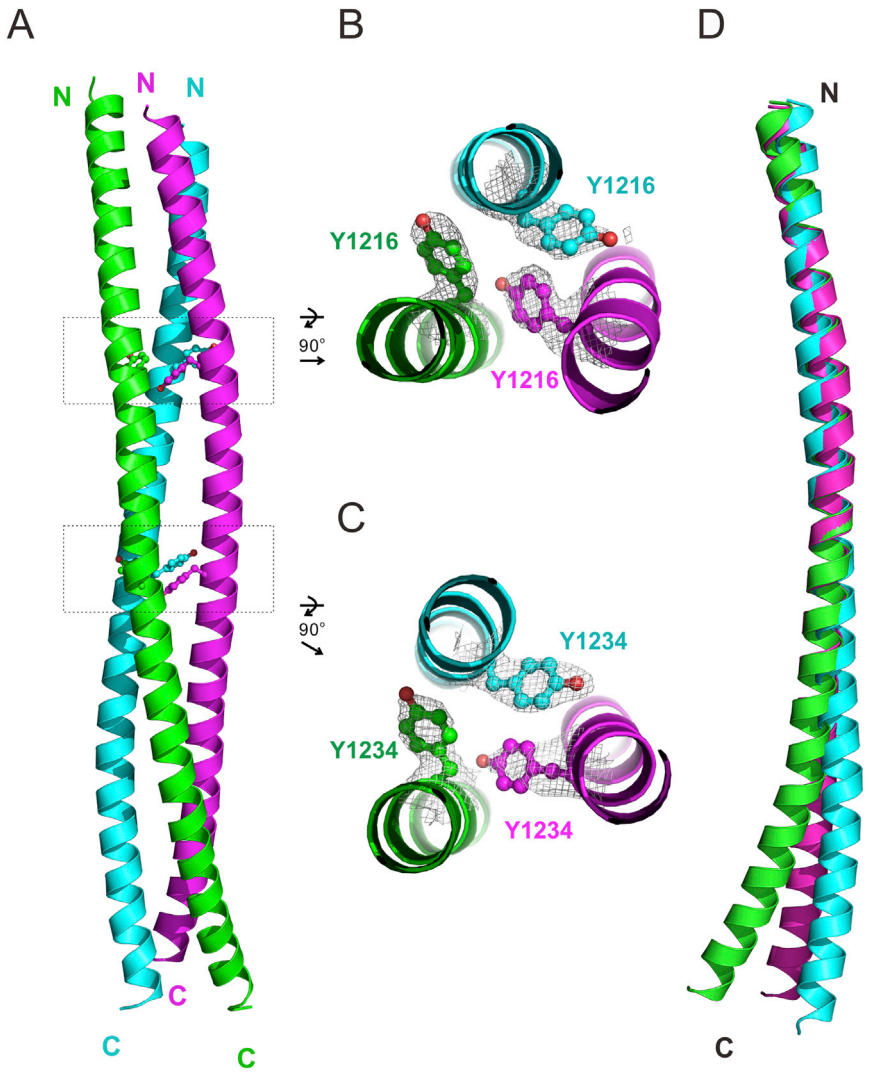

Figure S3. The SynGAP Coiled-Coil Trimer Is Overall Asymmetric, Related to Figure 2

(A) Ribbon presentation of the SynGAP coiled-coil trimer showing the sites of two asymmetric packing of Tyr residues (Y1216 and Y1234; indicated with dashed boxes) along the coiled-coil.

(B and C) 2Fc-Fo electron density map of the Tyr residues in the crystal structure showing the asymmetric arrangements of Y1216 and Y1234. The map is contoured at level of 1σ.

(D) Overlay of the N-termini of three helix chains of SynGAP coiled-coil trimer showing that the C-termini of the helices are not superimposed, illustrating that the three helices in the SynGAP coiled-coil trimer are not identical in their conformation.

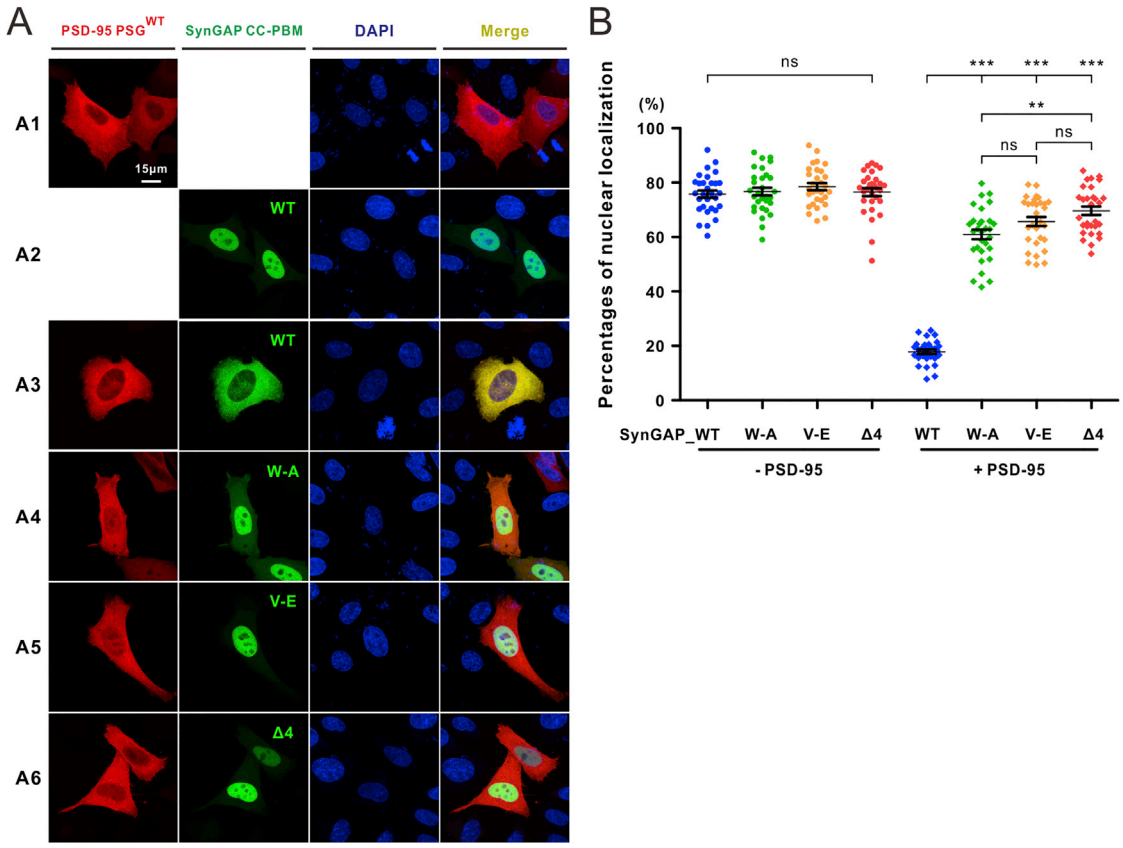

Figure S4. Co-localization of SynGAP CC-PBM and PSD-95 PSG in HeLa Cells, Related to Figure 3

(A) Representative images showing subcellular localizations of GFP-SynGAP CC-PBM (WT or various mutants) and RFP-PSD-95 PSG in HeLa cells when expressed individually or together. Nuclei were stained by DAPI.

(B) Quantification of nuclear-cytoplasmic distributions of SynGAP CC-PBM and its mutants in HeLa cells. A total of 30 cells from two independent cultures for each group were quantified and pooled for statistical analysis. The results are plotted as mean ± SEM. ***$p < 0.001$; **$p < 0.01$; ns, not significant using one-way ANOVA followed by Tukey's multiple comparison test.

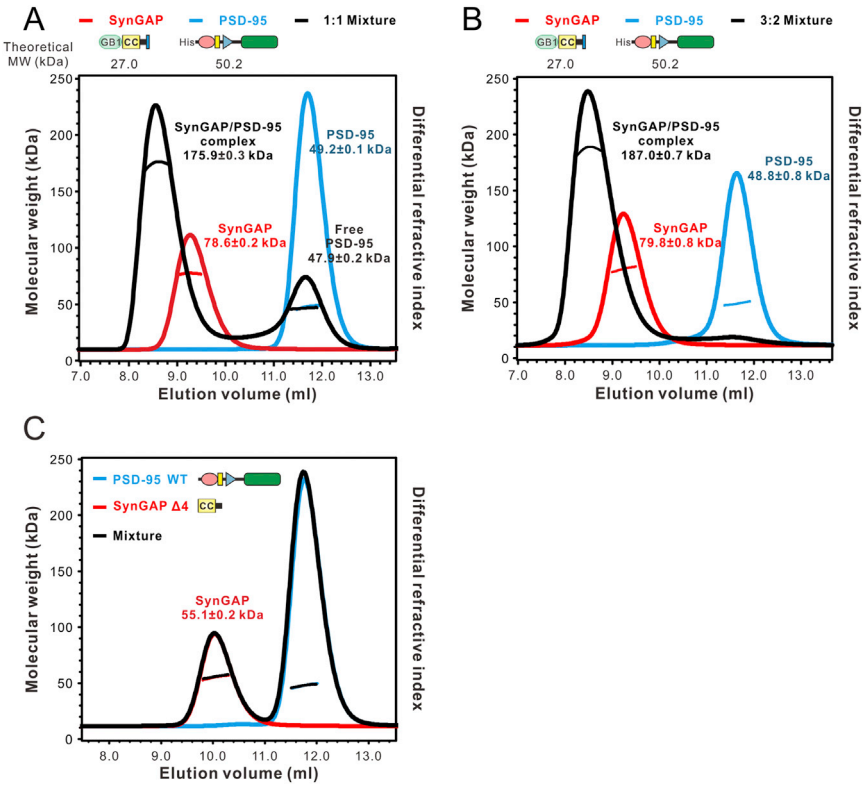

Figure S5. 3:2 Complex Formation between SynGAP CC-PBM and PSD-95 PSG, Related to Figure 3

(A) FPLC-coupled static light-scattering analysis showing the 3:2 complex (black curve) formed by mixing 100 μM GB1-tagged SynGAP CC-PBM (red curve) and 100 μM His-tagged PSD-95 PSG (cyan curve). A significant portion of PSD-95 (black curve) remained in its free form. The calculated molecular weights based on the scattering data are labeled in the figure and the theoretical molecular weights of the monomer units of these two proteins are indicated beneath the schematic domain diagram of each protein at the top of the figure.

(B) FPLC-coupled static light-scattering experiments showing a single peak (black curve) corresponding to the 3:2 complex formed by mixing 150 μM GB1-tagged SynGAP CC-PBM (red curve) with 100 μM His-tagged PSD-95 PSG (cyan curve).

(C) FPLC-coupled static light-scattering assay showing that deletion of the last 4 residues corresponding to the canonical PBM ("SynGAP CC-PBM Δ4") eliminated the interaction between SynGAP and PSD-95 PSG.

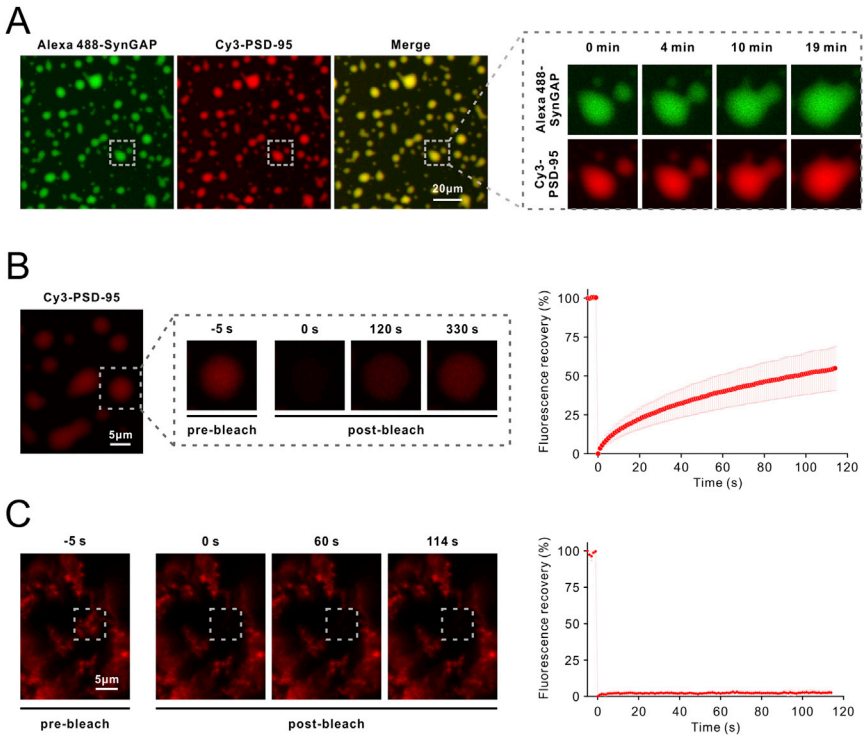

Figure S6. SynGAP CC-PBM/PSD-95 PSG Droplets In Vitro Showing Liquid-like Features and Undergoing Constant Molecular Exchanges, Related to Figure 4

(A) Co-localization of SynGAP and PSD-95 in the droplets with enriched concentrations. PSD-95 PSG and SynGAP CC-PBM (with affinity tags cleaved and removed) were prepared in buffer containing 50mM PBS pH7.4, 100mM NaCl, 5mM DTT. Alexa488 NHS ester (ThermoFisher) and Cy3 NHS ester (AAT Bioquest) were incubated with SynGAP or PSD-95 respectively at room temperature for 1h (fluorophore to protein molar ratio was 2:1, solution pH was adjusted by 100mM $NaHCO_3$ to pH8.3). Reaction was quenched by 200mM Tris pH8.3. Proteins were further purified into buffer with 50mM PBS pH7.4, 100mM NaCl, 5mM DTT by Hitrap desalting column. 1:1 mixture of Alexa488-SynGAP and Cy3-PSD-95 with 50 μM was observed in flow chamber at room temperature with a Zeiss LSM 880 confocal microscope. The enlarged images at right show the time-lapse images to demonstrate that small droplets can grow and merge into larger ones.

(B) FRAP analysis of Cy3-PSD-95 droplets in vitro assaying the exchange kinetics of the protein with the surrounding aqueous solution (1:1 mixture of unlabeled SynGAP and Cy3-labeled PSD-95 at 50 μM, room temperature). The Cy3 signal was bleached using a 561-nm laser beam. The red curve at right represents a FRAP recovery curve by averaging signals of 20 droplets with similar sizes each after photobleaching.

(C) FRAP analysis of Cy3-PSD-95 aggregates induced by heat denaturation, showing that proteins are not mobile in these aggregates. The flow chamber containing mixture as Panel B was sealed by nail polish, and then quickly subjected to a heat pulse to denature the two proteins in the chamber. The red curve at right is a FRAP recovery curve by averaging signal intensities of 5 different aggregates each after photobleaching. Time 0 refers to the time point right after the photobleaching pulse. All data are represented as mean ± SD.

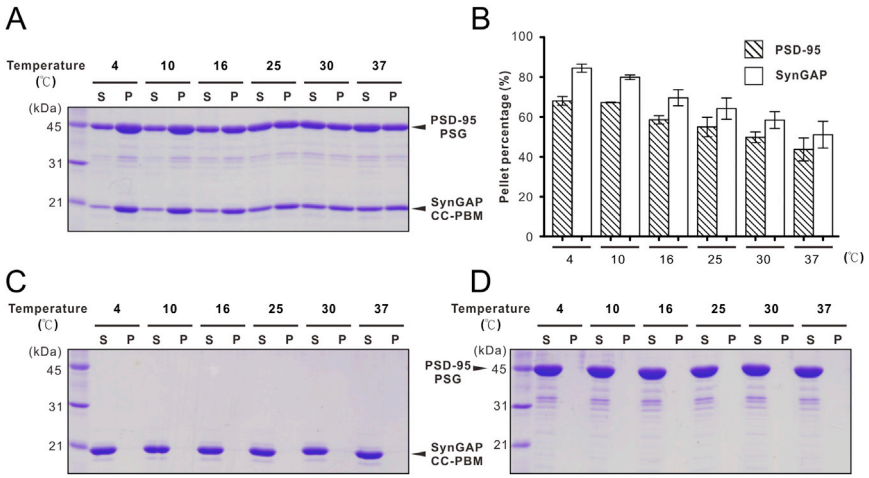

Figure S7. Temperature-Dependent Formation of the SynGAP/PSD-95 Complex Phase Transition, Related to Figure 4

(A and B) Lower temperature slightly favors the SynGAP/PSD-95 complex phase transition. In this experiment, 100 μM SynGAP CC-PBM, 100 μM PSD-95 PSG, and their 1:1 mixture at 100 μM were incubated in different temperatures (4°C, 10°C, 16°C, 25°C, 30°C, 37°C) for 10min (Eppendorf ThermoMixer C) before centrifugation at 16,873 g in the corresponding temperature for another 10min on a table-top temperature-controlled micro-centrifuge (Eppendorf Centrifuge 5418R). After centrifugation, aqueous solutions/supernatant and droplet phase/pellet were separated into two tubes. Pellets were washed once by buffer at the corresponding centrifugation temperature. Protein distributions were detected by SDS-PAGE and Coomassie blue staining. Quantitative data in Panel B represent results from three independent batches of sedimentation experiments and were plotted as mean ± SD.

(C and D) SynGAP and PSD-95 alone (each at 100 μM) are all in the supernatant at all temperatures assayed. Protein concentrations are calculated as their monomer units.